INSTITUTE OF PHYSICS PUBLISHING JOURNAL OF PHYSICS B: ATOMIC, MOLECULAR AND OPTICAL PHYSICS

J. Phys. B: At. Mol. Opt. Phys. **39** (2006) L35–L43 doi:10.1088/0953-4075/39/2/L03

LETTER TO THE EDITOR

Nondipole effects in double photoionization of He at 450 eV excess energy

Andrei Y Istomin[1], Anthony F Starace[1], N L Manakov[2], A V Meremianin[2], A S Kheifets[3] and Igor Bray[4]

[1] Department of Physics and Astronomy, The University of Nebraska, Lincoln, NE 68588-0111, USA
[2] Department of Physics, Voronezh State University, Voronezh 394006, Russia
[3] Research School of Physical Sciences and Engineering, Australian National University, Canberra, ACT 0200, Australia
[4] Centre for Atomic, Molecular and Surface Physics, School of Mathematical and Physical Sciences, Murdoch University, Perth 6150, Australia

Received 22 September 2005, in final form 13 November 2005
Published 19 December 2005
Online at stacks.iop.org/JPhysB/39/L35

Abstract

Convergent close-coupling results for the triply differential cross section for double photoionization of He that include dipole–quadrupole terms are shown to have improved agreement (as compared to dipole approximation results) with recent experiments using linearly polarized light (Knapp A *et al* 2005 *J. Phys. B: At. Mol. Opt. Phys.* **38** 615) for a number of kinematical configurations.

During the last decade, single-photon double ionization (DPI) of atoms and molecules has attracted much attention from both experimentalists and theorists. This was stimulated by the advent of VUV radiation sources that produce photons having well-defined polarization as well as by the development of techniques for coincidence measurements. Kinematically complete experiments allow one to gain much insight into the physical mechanisms of DPI by studying the photoelectron angular distributions described by the triply differential cross section (TDCS) [1–3]. Until recently, however, all experimental studies of the TDCS for DPI have been interpreted within the electric-dipole approximation (EDA) (see, e.g., recent experimental measurements [4–6] of the TDCS for DPI of He at excess energies of 100 eV and 450 eV with which convergent close-coupling (CCC) EDA predictions have been compared). Only recently have theoretical analyses of lowest order nondipole effects in the TDCS been reported [7–9]. The analytic analyses presented in these works have established the general angular-polarization structure of both the dipole–quadrupole transition amplitude and the TDCS for DPI from the $^1S_0$ two-electron bound state. The corresponding numerical analyses [7–9] have so far employed only a perturbative (in the interelectron interaction) dynamical model of the DPI process, whose gauge-invariant predictions for photon energies of the order of hundreds of eV are reliable only for large mutual ejection angles [8]. Thus, while predicting quite significant nondipole asymmetries in photoelectron angular distributions, the perturbative

numerical results in [7–9] call for confirmation by non-perturbative quantitative predictions of nondipole effects for comparisons with recent [4] and forthcoming measurements.

In this letter, we present numerical results within the CCC approach [10] for the TDCSs for DPI of He that include dipole–quadrupole terms for the case of the highest excess energy (450 eV) for which TDCS experimental data are available. We find that account of nondipole-induced asymmetries of the TDCS improves the agreement between theoretical predictions and recent experiments [4] for several kinematical configurations.

For DPI from the $^1S_0$ state to the final two-electron singlet state $|\mathbf{p}_1\mathbf{p}_2\rangle$ with asymptotic electron momenta $\mathbf{p}_1$ and $\mathbf{p}_2$, the TDCS that includes both dipole and the lowest order nondipole (quadrupole) terms can be written (in atomic units) as

$$\frac{\mathrm{d}^3\sigma}{\mathrm{d}\epsilon_1\,\mathrm{d}\Omega_1\,\mathrm{d}\Omega_2} = \mathcal{A}\{|A_\mathrm{d}|^2 + \mathrm{Re}(A_\mathrm{d}A_\mathrm{q}^*)\}, \tag{1}$$

where $\mathcal{A} = 4\pi^2\alpha p_1 p_2/\omega$ is a normalization factor and $\alpha = 1/137.036$. The dipole (A_d) and quadrupole (A_q) amplitudes have general representations (where $\mathbf{e}$ is the photon polarization vector, $(\mathbf{e}\cdot\mathbf{e}^*) = 1$, $(\mathbf{e}\cdot\mathbf{k}) = 0$ and $\mathbf{k} = (\omega/c)\hat{\mathbf{k}}$ is the photon wave vector) [9]

$$A_\mathrm{d} = f_1(\mathbf{e}\cdot\hat{\mathbf{p}}_1) + f_2(\mathbf{e}\cdot\hat{\mathbf{p}}_2), \tag{2}$$

$$A_\mathrm{q} = g_1(\mathbf{e}\cdot\hat{\mathbf{p}}_1)(\hat{\mathbf{p}}_1\cdot\hat{\mathbf{k}}) + g_2(\mathbf{e}\cdot\hat{\mathbf{p}}_2)(\hat{\mathbf{p}}_2\cdot\hat{\mathbf{k}}) + g_s[(\mathbf{e}\cdot\hat{\mathbf{p}}_1)(\hat{\mathbf{p}}_2\cdot\hat{\mathbf{k}}) + (\mathbf{e}\cdot\hat{\mathbf{p}}_2)(\hat{\mathbf{p}}_1\cdot\hat{\mathbf{k}})], \tag{3}$$

in terms of two dipole (f_1 and f_2) and three quadrupole (g_1, g_2 and g_s) polarization-invariant amplitudes. These amplitudes, in turn, are defined by a single function $f(p, p', \cos\theta)$ in the dipole case, $f_1 \equiv f(p_1, p_2, \cos\theta)$ and $f_2 \equiv f(p_2, p_1, \cos\theta)$ (where θ is the mutual ejection angle, $\cos\theta = (\hat{\mathbf{p}}_1\cdot\hat{\mathbf{p}}_2)$), and by two functions ($g(p, p', \cos\theta)$ and $g_s(p, p', \cos\theta)$) in the quadrupole case, $g_1 \equiv g(p_1, p_2, \cos\theta)$, $g_2 \equiv g(p_2, p_1, \cos\theta)$ and $g_s \equiv g_s(p_1, p_2, \cos\theta) = g_s(p_2, p_1, \cos\theta)$ (i.e., g_s is symmetric in p_1 and p_2). For both velocity and length gauges of the electron–photon interaction, the angular dependence of the functions $f(p, p', \cos\theta)$, $g(p, p', \cos\theta)$ and $g_s(p, p', \cos\theta)$ is parametrized by derivatives of the Legendre polynomial $P_l(x)$, $P_l^{(n)}(x) = (\mathrm{d}^n/\mathrm{d}x^n)P_l(x)$,

$$f(p, p', \cos\theta) = \sum_{l=1}^{\infty}(-1)^{l+1}\left[\sum_{l'=l\pm1} D_{ll'}(p, p')\right]P_l^{(1)}(\cos\theta), \tag{4}$$

$$g(p, p', \cos\theta) = \sum_{l=2}^{\infty}(-1)^{l}\left[\sum_{l'=l\pm2} Q_{ll'}(p, p') + \sqrt{6}Q_{ll}(p, p')\right]P_l^{(2)}(\cos\theta), \tag{5}$$

$$g_s(p, p', \cos\theta) = \sum_{l=1}^{\infty}(-1)^{l+1}\left[\sum_{l'=l\pm2} Q_{ll'}(p, p')P^{(2)}_{\frac{l+l'}{2}}(\cos\theta) + \sqrt{6}Q_{ll}(p, p')\left(P_{l+1}^{(2)}(\cos\theta) - \frac{2l+3}{2}P_l^{(1)}(\cos\theta)\right)\right], \tag{6}$$

where the energy-dependent dynamical factors $D_{ll'}(p, p')$ and $Q_{ll'}(p, p')$ are proportional to the reduced matrix elements of the dipole and quadrupole operators between the initial $^1S_0$-state and the P- and D-wave components of the final state $|\mathbf{pp}'\rangle$, with individual photoelectron angular momenta l and $l' = l \pm 1$ in $D_{ll'}(p, p')$, and l and $l' = l, l \pm 2$ in $Q_{ll'}(p, p')$ (see [9] for details). These dynamical factors are the only quantities that must be calculated numerically for a given photon frequency and excess energy sharing within any particular dynamical model of DPI in order to reconstruct the dipole–quadrupole TDCS for any experimental geometry

Table 1. Dipole and quadrupole DPI matrix elements, $D_{l_1 l_2}(E_1, E_2)$ and $Q_{l_1 l_2}(E_1, E_2)$ (cf equations (4)–(6)), for $E_1 = 50$ eV and $E_2 = 400$ eV.

$D_{l_1 l_2} = \lvert D_{l_1 l_2}\rvert \exp(\mathrm{i}\varphi_\mathrm{d})$				$Q_{l_1 l_2} = \lvert Q_{l_1 l_2}\rvert \exp(\mathrm{i}\varphi_\mathrm{q})$			
l_1	l_2	$\lvert D_{l_1 l_2}\rvert$ (10^{-5} au)	φ_d (rad)	l_1	l_2	$\lvert Q_{l_1 l_2}\rvert$ (10^{-7} au)	φ_q (rad)
0	1	16.2737	−2.2951	0	2	71.5571	0.4281
1	0	7.4483	−3.0262	1	1	26.2991	1.4531
1	2	4.3887	−0.9795	2	0	19.0392	−1.4822
2	1	4.5346	−2.0681	1	3	6.7524	0.5346
2	3	3.3087	0.3911	2	2	11.0914	1.3526
3	2	2.3107	−0.8404	3	1	6.9557	−0.9733
3	4	1.7939	1.4008	2	4	3.0325	−2.5947
4	3	0.7855	0.3753	3	3	3.1639	1.9405
4	5	0.5329	2.4977	4	2	1.1233	0.8349
5	4	0.5027	1.5894	3	5	2.1564	−2.0879
5	6	0.3927	−2.6553	4	4	0.6136	−2.9847
6	5	0.2964	2.8282	5	3	0.3854	2.3114
				4	6	0.4793	−1.0953
				5	5	0.2927	−1.7472
				6	4	0.2753	−2.6901
				6	6	0.1663	−0.5368

and for any polarization state of the photon beam (cf table 1). In order to calculate $D_{ll'}(p, p')$ and $Q_{ll'}(p, p')$ in the present letter, we have used the CCC approach [10] to describe the two-electron continuum state $|\mathbf{pp}'\rangle$, while the He ground state is described by a multi-configuration Hartree–Fock wavefunction. The procedure for evaluating $D_{ll'}(p, p')$ and $Q_{ll'}(p, p')$ is the same as that employed in [11]. In brief, these matrix elements are calculated as the optical limit, $q \to 0$, of the matrix elements of the multipole expansion components of the Born operator, $\mathrm{e}^{\mathrm{i}\mathbf{q}\cdot\mathbf{r}}$, that have been calculated within the CCC approach for study of the (e, 3e) process in He [12].

In figures 1–5, we present velocity gauge CCC results for the TDCS of DPI by linearly polarized light ($\mathbf{e} = \mathbf{e}^* \equiv \hat{\epsilon}$) for an excess energy of 450 eV, calculated both within the EDA (dashed curves) and also taking into account the lowest order nondipole corrections (full curves). In all figures, it is assumed that the photon wave vector $\mathbf{k}$ points downward. (The direction of $\mathbf{k}$ in the experiment [4] has not been determined [14].)

Figure 1 compares our present CCC predictions with prior LOPT results [9]. One sees that despite the scaling of the LOPT results by a factor of 0.4 in the right half plane, there still exists disagreement between these two theories within the EDA, especially in the region of small mutual angles, thereby indicating the importance of high-order electron correlations [9, 13]. However, the relative magnitudes of the lowest order nondipole corrections in both LOPT and CCC methods are in reasonable agreement.

Figures 2–5 present comparisons of our present EDA and nondipole CCC predictions with experiment for all kinematical configurations used in [4], i.e., for four energy sharings and, for each energy sharing, for three different ejection angles of one of the photoelectrons. Figure 2 shows the results for the least asymmetric energy sharing presented in [4], when one electron has an energy of 50 eV and the second electron has an energy of 400 eV. When one electron is ejected along the photon polarization direction (i.e., $\theta_1 = 0^\circ$), the angular distribution of the second electron must be symmetric about this direction, provided that nondipole effects are negligible. One sees, however, that when it is the *slow* electron that is ejected along the

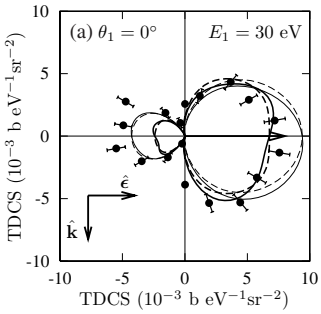

Figure 1. Polar plots of the TDCS for DPI of He at an excess energy of 450 eV for the case of linearly polarized light. The photon wave vector **k** and polarization $\hat{\epsilon}$ are assumed to be directed as shown. The electron having energy E_1 is ejected at an angle $\theta_1 = 0°$ with respect to $\hat{\epsilon}$. The angular distribution of the second electron is plotted versus polar angle θ_2. Bold curves: CCC; curves of regular thickness: LOPT [9] (for $\theta_2 < 90°$ and $270° < \theta_2 < 360°$, LOPT results were multiplied by a factor of 0.4 for ease of comparison). Full curves: dipole–quadrupole results; dashed curves: EDA results. Dots with error bars: experimental data [4] (normalized to the CCC results).

photon polarization direction (i.e., the case of $E_1 = 50$ eV and $\theta_1 = 0°$ shown in figure 2(a)), the experimental data exhibit a significant asymmetry with respect to the photon polarization axis: for $0° < \theta_2 < 90°$ and $270° < \theta_2 < 360°$ the angular distribution of the faster electron is shifted downward, while for $90° < \theta_2 < 270°$ it is shifted upward. One sees that our TDCS results that include nondipole corrections in figure 2(a) precisely reproduce this asymmetry of the experimental data. In the case when the *faster* electron is ejected along the photon polarization direction (see figure 2(d)), no distinct asymmetry is seen in the experimental data to within the error bars. Our TDCS results for this case exhibit only a small asymmetry, which however is qualitatively different from that in figure 2(a): the entire angular distribution is shifted downward.

For geometries in which one of the electrons is ejected at a fixed nonzero angle θ_1 (see figures 2(b), (c), (e) and (f)), identification of nondipole asymmetries in the present experimental data is impossible, as the shapes of angular distributions that are unaffected by nondipole effects are unknown. The shapes of such angular distributions may be determined, however, in an experiment where both electrons are detected in the plane perpendicular to the photon beam direction (i.e., using the *perpendicular plane geometry*), since in this case the lowest order nondipole corrections do not contribute [7]. Comparison of the TDCS measurements performed in the *coplanar geometry* (as in [4]) and in the *perpendicular plane geometry* (as in [5], but still using linearly polarized light) would thus provide the possibility of identifying nondipole effects even for a nonzero angle θ_1. Our CCC results in figures 2(b), (c), (e) and (f) provide numerical predictions for the shapes of such angular distributions. One sees that for $\theta_1 = 45°$, when the ejection direction of the *slower* electron is fixed, the magnitude of the TDCS lobe in the angular range $90° < \theta_2 < 270°$ is decreased by the nondipole effects, while the lobe that lies in the ranges $0° < \theta_2 < 90°$ and $270° < \theta_2 < 360°$ is increased by the nondipole effects. When the ejection direction of the *faster* electron is fixed, the magnitude of both TDCS lobes is decreased. For $\theta_1 = 90°$, one sees that when the ejection direction of the slower electron is fixed, both TDCS lobes are shifted downward due to nondipole effects. When the ejection direction of the faster electron is fixed at $\theta_1 = 90°$, account of nondipole effects leads to a significant decrease in the size of both TDCS lobes.

In figures 3–5, we present our dipole and nondipole TDCS results for three other energy sharings and compare them with the corresponding experimental data [4]. In figure 3(a), there

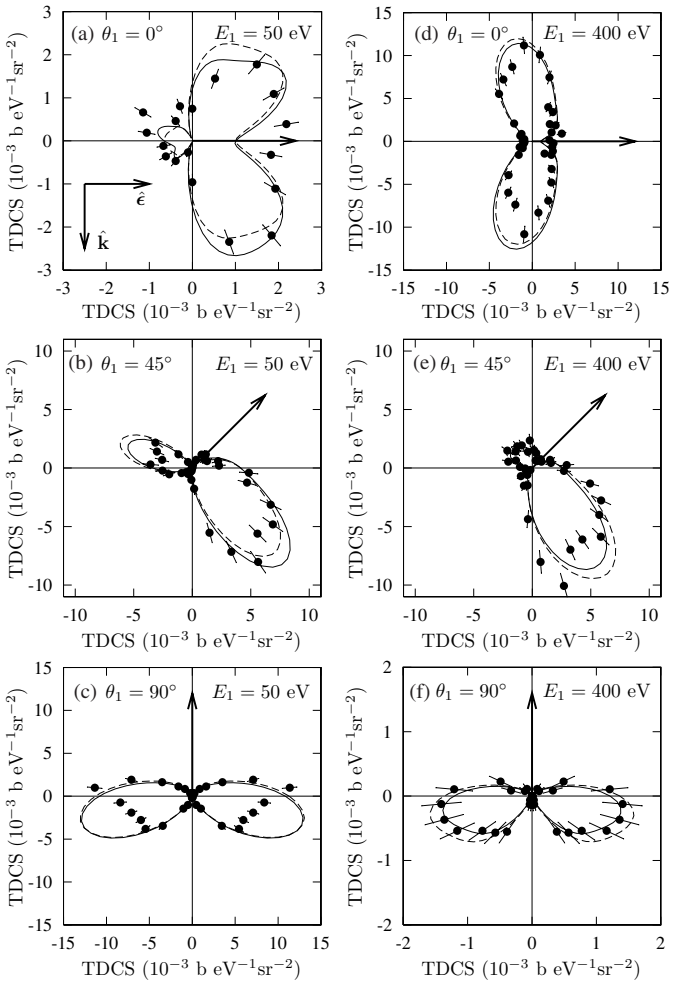

Figure 2. Polar plots of the TDCS for DPI of He at an excess energy of 450 eV for the case of linearly polarized light. The photon wave vector **k** and polarization $\hat{\epsilon}$ are assumed to be directed as in (a). The two electrons are ejected with energies of 50 eV and 400 eV. The electron having energy E_1 is ejected at an angle θ_1 with respect to the photon polarization, as shown by the arrow. The angular distribution of the second electron is plotted versus polar angle θ_2. Full curves: dipole–quadrupole CCC results; dashed curves: EDA CCC results. Dots with error bars: experimental data [4] (normalized to the CCC results).

is asymmetry in the experimental data that is qualitatively similar to that in figure 2(a) described above, and it is well reproduced by our nondipole TDCS results (while our EDA results in figure 3(a) differ from the experimental data in a way that is similar to the corresponding differences seen in figure 2(a)). The nondipole asymmetries in our predictions for other ejection angles ($\theta_1 = 45°$ and $\theta_1 = 90°$) in figures 3–5 are similar to those in figure 2 with one exception: as the energy sharing becomes more asymmetric (cf figures 4 and 5), the account of nondipole corrections results in the downward shift of both lobes in the angular distributions of the faster electron. Our nondipole TDCSs in figures 3(a) and 5(a) agree qualitatively with those predicted in [9].

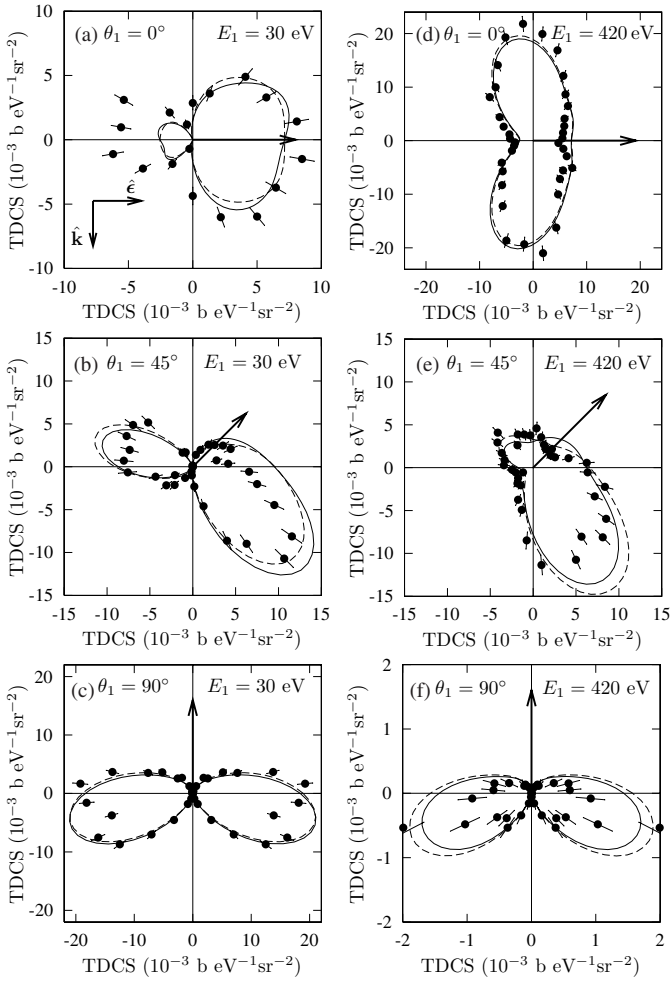

Figure 3. Same as figure 2, except that the electrons are ejected with energies 30 eV and 420 eV.

In figures 2–5, the relative magnitude of nondipole effects for each fixed energy sharing depends sensitively on θ_1. The largest nondipole effects are found for angles θ_1 for which the dipole TDCS is small (cf figures 2(a) and (f), 4(f) and 5(f)) and vice versa (cf figures 2(c), 4(d) and 5(a) and (d)). This indicates that while the interference of dipole amplitudes in the EDA TDCS is rather sensitive to θ_1, the dipole–quadrupole interference terms (which cause the lowest order nondipole effects) have little sensitivity to the value of this angle[5].

In table 1, we present numerical values of the matrix elements $D_{l_1 l_2}$ and $Q_{l_1 l_2}$ up to $l = 6$ for the energy sharing configuration in which the most pronounced nondipole effects have been found, i.e., for $E_1 = 50$ eV and $E_2 = 400$ eV (cf figure 2(a)). These matrix elements allow one to reconstruct all the dipole–quadrupole TDCSs shown in figure 2, as well as TDCSs at this energy sharing for an arbitrary photon polarization and kinematical configuration. (Note

[5] This difference in sensitivity may be explained (in part) by considering that the EDA terms involve a factor $(\hat{\mathbf{p}}_1 \cdot \mathbf{e})$, which decreases as θ_1 varies from 0° to 90°. The dipole–quadrupole terms also include this factor, but in addition have a factor $(\hat{\mathbf{p}}_1 \cdot \hat{\mathbf{k}})$, which increases as θ_1 varies from 0° to 90°, thus making the dipole–quadrupole terms less sensitive to the value of θ_1. See equations (10)–(12) of [7].

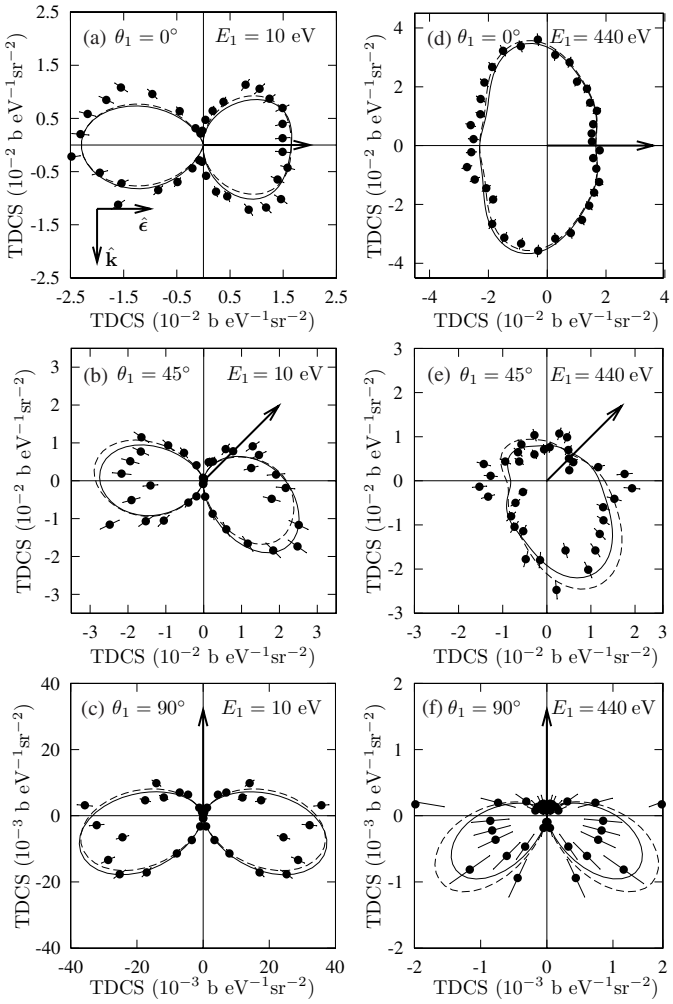

Figure 4. Same as figure 2, except that the electrons are ejected with energies 10 eV and 440 eV.

that the TDCSs in figures 2(d)–(f) can be reconstructed by interchanging l_1 and l_2 in the matrix elements in table 1.)

To conclude, we have presented the first accurate calculations of the DPI TDCSs including lowest order nondipole corrections. For the case of not too extreme asymmetric energy sharing and ejection of the *slower* electron along the photon polarization direction, the angular distributions of the *faster* electron exhibit asymmetries that agree well with those seen in the experimental data for this geometrical configuration. This indicates the importance of nondipole effects in coincidence measurements that use coplanar geometry at photon energies as low as a few hundred electron volts. The assessment of the importance of nondipole effects in the experimental data for nonzero θ_1 requires additional measurements done in the *perpendicular plane geometry* (in which the lowest order nondipole effects vanish) so that one may compare results to those measured in *coplanar geometry* as well as to our nondipole and EDA predictions.

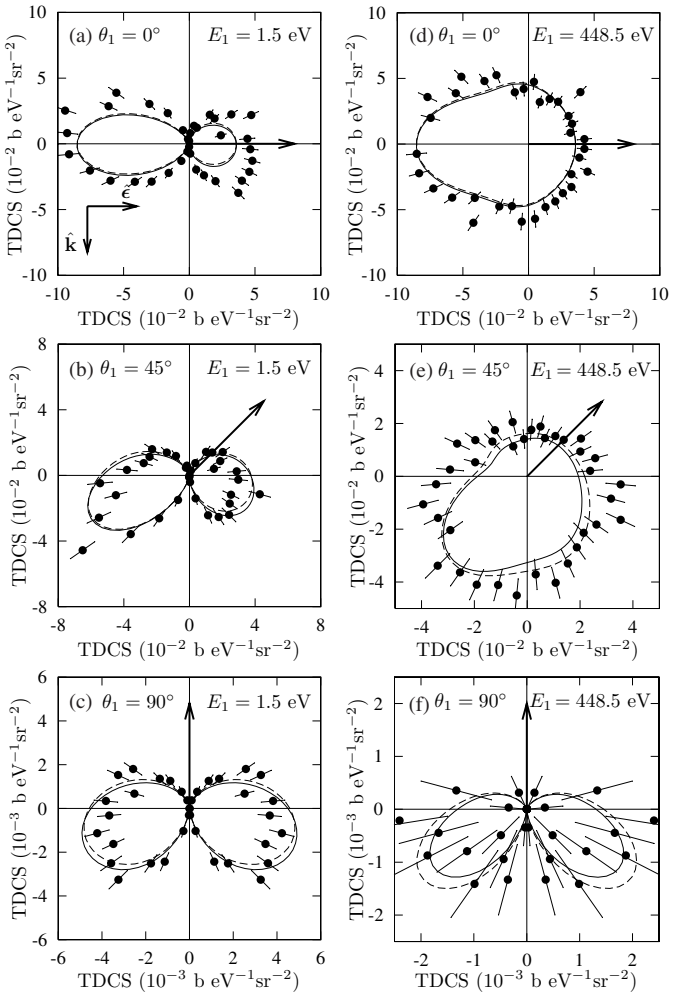

Figure 5. Same as figure 2, except that the electrons are ejected with energies 1.5 eV and 448.5 eV.

Acknowledgments

We wish to thank A Knapp and R Dörner for providing us with their data. This work was supported in part by the US Department of Energy, Office of Science, Division of Chemical Sciences, Geosciences and Biosciences, under grant DE-FG03-96ER14646, by RFBR grant 04-02-16350 and by the joint grant VZ-010-0 of the CRDF and the RF Ministry of Education and Sciences (NLM and AVM). The CCC computations presented in this letter were performed using the Compaq AlphaServer SC National Facility of the Australian Partnership for Advanced Computing.

References

[1] Briggs J S and Schmidt V 2000 *J. Phys. B: At. Mol. Opt. Phys.* **33** R1
[2] King G C and Avaldi L 2000 *J. Phys. B: At. Mol. Opt. Phys.* **33** R215

[3] Avaldi L and Huetz A 2005 *J. Phys. B: At. Mol. Opt. Phys.* **38** S861
[4] Knapp A *et al* 2005 *J. Phys. B: At. Mol. Opt. Phys.* **38** 615
[5] Knapp A *et al* 2005 *J. Phys. B: At. Mol. Opt. Phys.* **38** 635
[6] Knapp A *et al* 2005 *J. Phys. B: At. Mol. Opt. Phys.* **38** 645
[7] Istomin A Y, Manakov N L, Meremianin A V and Starace A F 2004 *Phys. Rev. Lett.* **92** 063002
[8] Istomin A Y, Manakov N L, Meremianin A V and Starace A F 2004 *Phys. Rev.* A **70** 010702
[9] Istomin A Y, Manakov N L, Meremianin A V and Starace A F 2005 *Phys. Rev.* A **71** 052702
[10] Kheifets A S and Bray I 1998 *Phys. Rev.* A **57** 2590
[11] Istomin A Y, Starace A F, Manakov N L, Meremianin A V, Kheifets A S and Bray I 2005 *Phys. Rev.* A **72** 052708
[12] Kheifets A S and Bray I 2004 *Phys. Rev.* A **69** 050701
[13] Istomin A Y, Manakov N L and Starace A F 2004 *Phys. Rev.* A **69** 032713
[14] Knapp A 2005 Private communication